Proton-proton bremsstrahlung: Consequences of different on-shell-point conditions

Yi Li
College of Physics and Technology, Guangxi University, Nanning, Guangxi 530004, People's Republic of China

M. K. Liou
Department of Physics and Institute for Nuclear Theory, Brooklyn College of the City University of New York, Brooklyn, New York 11210, USA

W. M. Schreiber
Department of Physics, College of Staten Island of the City University of New York, Staten Island, New York 10314, USA

B. F. Gibson
Theoretical Division, Los Alamos National Laboratory, Los Alamos, New Mexico 87545, USA
(Received 22 July 2011; published 19 September 2011)

Background: Proton-proton bremsstrahlung ($pp\gamma$) is investigated both theoretically and experimentally. The $pp\gamma$ amplitudes can be classified according to the number and location of on-shell points at which they are evaluated. Quantitative understanding of the effect on the $pp\gamma$ cross section of using different on-shell-point conditions is lacking, but it is essential to identifying the photon emission mechanism governing the $pp\gamma$ process. **Method**: Four different $pp\gamma$ amplitudes, which include four-on-shell-point amplitudes and one-on-shell-point amplitude, are generated from a realistic one-boson-exchange (ROBE) model for pp scattering. These ROBE amplitudes are used to investigate the consequence of using different on-shell-point conditions in calculating the $pp\gamma$ cross sections. **Purpose**: We verify the validity of the ROBE $pp\gamma$ amplitudes. We explore similarities between the four-on-shell-point ROBE and two-u-two-t special (TuTts) soft-photon $pp\gamma$ amplitudes and important differences with the one-on-shell-point ROBE and Low $pp\gamma$ amplitudes. We demonstrate that the precision Kernfysisch Versneller Instituut (KVI) data can only be described by the four-on-shell-point (ROBE or TuTts) amplitude. We use the ROBE four-on-shell-point amplitude and one-on-shell-point amplitude to investigate systematically the effect of using different on-shell-point conditions to calculate the $pp\gamma$ cross section. Furthermore, we identify a general principle that governs the process. This general principle is also applicable to other bremsstrahlung processes involving the scattering of two identical nucleons. **Results**: (i) The four-on-shell-point ROBE (or TuTts) amplitude describes the high-precision KVI data much better than does the one-on-shell-point ROBE (or Low) amplitude. Although the contribution from the anomalous magnetic moment of the proton is very significant, it does not completely dominate the KVI $pp\gamma$ cross sections. (ii) The four-on-shell-point ROBE (or TuTts) amplitude describes the TRIUMF data better than does the one-on-shell-point ROBE (or Low) amplitude. (iii) The effect on the $pp\gamma$ cross section of using different on-shell-point conditions is significant in the hard-photon region, i.e., for small proton scattering angles θ ($=\theta_3 = \theta_4$, symmetric scattering angles) far from the elastic limit ($\theta \to 45^\circ$); in contrast, the effect becomes insignificant in the vicinity of the elastic limit. Near the limit as θ tends to 45° (or as the photon energy K approaches zero), the four-on-shell-point and one-on-shell-point amplitudes approach one another, a general principle applicable to all bremsstrahlung processes because only kinematics is involved. **Conclusion**: The four-on-shell-point ROBE amplitude provides a quantitative description of $pp\gamma$ cross sections. The anomalous magnetic moment is an important component of the photon emission mechanism. The four-on-shell-point property of the full ROBE amplitude is essential to properly describing the complete range of the precision KVI data and the TRIUMF data, although the one-on-shell-point ROBE amplitude is adequate in the region near the elastic limit.

DOI: 10.1103/PhysRevC.84.034007 PACS number(s): 25.40.−h, 13.40.−f, 13.75.Gx, 13.60.−r

I. INTRODUCTION

Any valid nuclear bremsstrahlung amplitude must be gauge invariant and consistent with the soft-photon theorem [1,2]. In addition to these two fundamental requirements, the amplitudes for certain bremsstrahlung processes must satisfy additional theoretical constraints. For example, the bremsstrahlung amplitudes that involve two identical fermions (spin-$\frac{1}{2}$ particles) must also satisfy the Pauli principle. Furthermore, because the soft-photon theorem does not specify the on-shell points at which the bremsstrahlung amplitude can be evaluated (see the appendix of Ref. [3] for a detailed discussion), different bremsstrahlung amplitudes (evaluated at different on-shell points) can be constructed. As discussed in Sec. II, three different on-shell-point conditions can be defined for a given bremsstrahlung process. This implies that at least three different bremsstrahlung amplitudes can be constructed for the process. This theoretical ambiguity cannot be ignored. It is essential to investigate the effect on the bremsstrahlung cross

section of using different on-shell-point conditions, because the details will enhance our understanding of the photon emission mechanism governing the bremsstrahlung process.

The proton-proton bremsstrahlung ($pp\gamma$) process,

$$p(p_1^\mu) + p(p_2^\mu) \to p(p_3^\mu) + p(p_4^\mu) + \gamma(K^\mu), \qquad (1)$$

has been investigated both theoretically and experimentally. Precise experimental data are available in a wide energy range (see Ref. [3] for an extensive list of references). These data, especially the high-precision $pp\gamma$ data from the Kernfysisch Versneller Instituut (KVI) experiment [4–7] and the TRIUMF $pp\gamma$ data at 280 MeV [8], were used to explore the validity of various $pp\gamma$ amplitudes. We identified optimum $pp\gamma$ amplitudes that describe the measured $pp\gamma$ data. In a recent investigation [9,10], two relativistic amplitudes, Low's amplitude $M_\mu^{\rm Low}$ [11] and a two-u-two-t special (TuTts) amplitude $M_\mu^{\rm TuTts}$ [12,13], were used to compare with the KVI data. These amplitudes were also used to study the effect of nucleon anomalous magnetic moments in nucleon-nucleon bremsstrahlung ($NN\gamma$, including $pp\gamma$, $np\gamma$, and $nn\gamma$). Both amplitudes, $M_\mu^{\rm TuTts}$ and $M_\mu^{\rm Low}$, are gauge invariant and obey the soft-photon theorem. However, $M_\mu^{\rm TuTts}$ and $M_\mu^{\rm Low}$ differ significantly: The amplitude $M_\mu^{\rm TuTts} \equiv M_\mu^{\rm TuTts}(\Gamma_\mu; u_{41}, u_{32}, t_{31}, t_{42})$ [$t_{ij} = (p_i - p_j)^2$ ($ij = 31, 42$) and $u_{ik} = (p_i - p_k)^2$ ($ik = 41, 32$) are Mandelstam variables] is evaluated at four different on-shell points, whereas the amplitude $M_\mu^{\rm Low} \equiv M_\mu^{\rm Low}(\Gamma_\mu; \bar{u}, \bar{t})$ [$\bar{t} = (t_{31} + t_{42})/2$ and $\bar{u} = (u_{41} + u_{32})/2$] is evaluated at a single, unique on-shell point. The results obtained from Refs. [9,10] demonstrate that the KVI cross-section data can only be described by the four-on-shell-point amplitude $M_\mu^{\rm TuTts}$. This illustrates that the effect of evaluating the $pp\gamma$ cross section at different on-shell points is significant. The results from Ref. [10] also reveal that in contrast the effect in the $np\gamma$ cross section is insignificant, because the leading-term cancellation in the identical-particle $pp\gamma$ process, which makes the anomalous magnetic moment contribution significant, does not occur in the nonidentical-particle $np\gamma$ process.

We investigate here the effect of using different on-shell-point conditions in evaluating the $pp\gamma$ cross section. To demonstrate that this should be independent of the bremsstrahlung approach used, we employ an alternative realistic one-boson-exchange (ROBE) amplitude in this work. Our investigation using the ROBE approach confirms that the four-on-shell-point amplitude is required to describe those KVI data discussed in Refs. [9,10]. Furthermore, on the basis of our numerical calculations as well as an analytic proof, we establish a general principle regarding the effect of different on-shell-point conditions on the $pp\gamma$ cross section that in the elastic limit the four-on-shell-point amplitude and one-on-shell-point amplitude become the same. This is an important characteristic of the fundamental photon emission mechanism governing the $pp\gamma$ process. Even though the $pp\gamma$ process was used to investigate the effect of different on-shell-point conditions, the results of this investigation can also be applied to other bremsstrahlung processes that involve the scattering of two identical nucleons, such as the $nn\gamma$, $pp\nu\bar{\nu}$, and $nn\nu\bar{\nu}$ processes.

This paper is organized as follows. In Sec. II we define three different sets of on-shell points. In Sec. III we define four different ROBE $pp\gamma$ amplitudes used to calculate the $pp\gamma$ cross sections. In Sec. IV we compare the calculated $pp\gamma$ cross sections using the ROBE amplitudes with (i) the KVI data and the TRIUMF data and (ii) the $pp\gamma$ cross sections calculated using the amplitudes $M_\mu^{\rm TuTts}$ and $M_\mu^{\rm Low}$. In Sec. V we define the ratio $R_{\psi_\gamma}^{E_i}$ for a given incident proton energy E_i, the value of the cross section at ψ_γ calculated using the four-on-shell-point amplitude divided by the value of the cross section at ψ_γ calculated from the one-on-shell-point amplitude. This ratio can be written as a function of the proton scattering angle $\theta = \theta_3 = \theta_4$ or as a function of the photon energy K, i.e., $R_{\psi_\gamma}^{E_i}(\theta)$ or $R_{\psi_\gamma}^{E_i}(K)$. We utilize both $R_{\psi_\gamma}^{E_i}(\theta)$ and $R_{\psi_\gamma}^{E_i}(K)$ to investigate the result of using different on-shell-point conditions on the $pp\gamma$ cross section. Our conclusions are summarized in Sec. VI. In the Appendix, we prove that $\lim_{K\to 0} R_{\psi_\gamma}^{E_i}(K) = 1$. Thus, we demonstrate that $\lim_{\theta\to 45^\circ} R_{\psi_\gamma}^{E_i}(\theta) = \lim_{K\to 0} R_{\psi_\gamma}^{E_i}(K) = 1$, independent of E_i and ψ_γ.

II. THREE SETS OF ON-SHELL POINTS

A. Mandelstam variables

The following Mandelstam variables can be used to define three sets of on-shell points for the $pp\gamma$ process, Eq. (1):

$$\begin{aligned}
t_{31} &= (p_3 - p_1)^2 = t_{13},\\
t_{42} &= (p_4 - p_2)^2 = t_{24},\\
u_{41} &= (p_4 - p_1)^2 = u_{14},\\
u_{32} &= (p_3 - p_2)^2 = u_{23},\\
s_i &= (p_1 + p_2)^2,\\
s_f &= (p_3 + p_4)^2,\\
\bar{t} &= \tfrac{1}{2}(t_{31} + t_{42}) = \tfrac{1}{2}(t_{13} + t_{24}),\\
\bar{u} &= \tfrac{1}{2}(u_{41} + u_{32}) = \tfrac{1}{2}(u_{14} + u_{23}),\\
\bar{s} &= \tfrac{1}{2}(s_i + s_f),\\
\tilde{t} &= \lim_{K\to 0} \bar{t} = \lim_{K\to 0} t_{31} = \lim_{K\to 0} t_{42},\\
\tilde{u} &= \lim_{K\to 0} \bar{u} = \lim_{K\to 0} u_{41} = \lim_{K\to 0} u_{32},\\
\tilde{s} &= \lim_{K\to 0} \bar{s} = \lim_{K\to 0} s_f.
\end{aligned} \qquad (2)$$

B. The first set: The four on-shell points

The $pp\gamma$ process involves four proton legs. Because a photon can be emitted from any one of these four legs, the following four independent $pp\gamma$ amplitudes can be defined.

(i) If the photon is emitted from the p_1 leg, the bremsstrahlung amplitude $M_\mu^{P_1}(\Gamma_\mu; u_{32}, t_{42})$ evaluated at the on-shell point (u_{32}, t_{42}) can be defined. This on-shell point satisfies the on-shell point condition

$$s_{22} + u_{32} + t_{42} = 4m^2, \qquad (3a)$$

where m is the proton mass and

$$s_{22} = s_f + 2p_1 \cdot K. \qquad (4a)$$

(ii) If the photon is emitted from the p_2 leg, the bremsstrahlung amplitude $M_\mu^{P_2}(\Gamma_\mu; u_{41}, t_{31})$ evaluated at the on-shell point (u_{41}, t_{31}) can be defined. This on-shell point satisfies the on-shell point condition

$$s_{11} + u_{41} + t_{31} = 4m^2, \tag{3b}$$

where m is the proton mass and

$$s_{11} = s_f + 2p_2 \cdot K. \tag{4b}$$

(iii) If the photon is emitted from the p_3 leg, the bremsstrahlung amplitude $M_\mu^{P_3}(\Gamma_\mu; u_{41}, t_{42})$ evaluated at the on-shell point (u_{41}, t_{42}) can be defined. This on-shell point satisfies the on-shell point condition

$$s_{12} + u_{41} + t_{42} = 4m^2, \tag{3c}$$

where m is the proton mass and

$$s_{12} = s_i - 2p_3 \cdot K. \tag{4c}$$

(iv) If the photon is emitted from the p_4 leg, the bremsstrahlung amplitude $M_\mu^{P_4}(\Gamma_\mu; u_{32}, t_{31})$ evaluated at the on-shell point (u_{32}, t_{31}) can be defined. This on-shell point satisfies the on-shell point condition

$$s_{21} + u_{32} + t_{31} = 4m^2, \tag{3d}$$

where m is the proton mass and

$$s_{21} = s_i - 2p_4 \cdot K. \tag{4d}$$

The total emission process is the sum of the emission processes from the four proton legs. Therefore, the total bremsstrahlung amplitude, which is the TuTts type, can be written as

$$\begin{aligned} &M_\mu^{\mathrm{TuTts}}(\Gamma_\mu; u_{41}, u_{32}, t_{31}, t_{42}) \\ &\quad = M_\mu^{P_1}(\Gamma_\mu; u_{32}, t_{42}) + M_\mu^{P_2}(\Gamma_\mu; u_{41}, t_{31}) \\ &\qquad + M_\mu^{P_3}(\Gamma_\mu; u_{41}, t_{42}) + M_\mu^{P_4}(\Gamma_\mu; u_{32}, t_{31}). \end{aligned} \tag{5}$$

The amplitude $M_\mu^{\mathrm{TuTts}}(\Gamma_\mu; u_{41}, u_{32}, t_{31}, t_{42})$ is evaluated at four different on-shell points $[(u_{32}, t_{42}), (u_{41}, t_{31}), (u_{41}, t_{42}), (u_{32}, t_{31})]$ whose respective conditions are given by Eqs. (3a), (3b), (3c), and (3d). We emphasize that the choice of the four separate on-shell points at which to evaluate the amplitude $M_\mu^{\mathrm{TuTts}}(\Gamma_\mu; u_{41}, u_{32}, t_{31}, t_{42})$ is not only natural but also physical. Note that we can also write

$$\begin{aligned} M_\mu^{P_1}(\Gamma_\mu; u_{32}, t_{42}) &= M_\mu^{P_1}(\Gamma_\mu; s_{22}, t_{42}), \\ M_\mu^{P_2}(\Gamma_\mu; u_{41}, t_{31}) &= M_\mu^{P_2}(\Gamma_\mu; s_{11}, t_{31}), \\ M_\mu^{P_3}(\Gamma_\mu; u_{41}, t_{42}) &= M_\mu^{P_3}(\Gamma_\mu; s_{12}, t_{42}), \\ M_\mu^{P_4}(\Gamma_\mu; u_{32}, t_{31}) &= M_\mu^{P_4}(\Gamma_\mu; s_{21}, t_{31}), \end{aligned} \tag{6}$$

C. The second set: The one on-shell point $(\bar{u}, \bar{t})$

If we add all four conditions given by Eqs. (3a)–(3d), we find

$$\bar{s} + \bar{u} + \bar{t} = 4m^2 + \tfrac{1}{2}(p_3 \cdot K + p_4 \cdot K - p_1 \cdot K - p_2 \cdot K). \tag{7}$$

Using the energy-momentum conservation condition

$$p_1^\mu + p_2^\mu = p_3^\mu + p_4^\mu + K^\mu, \tag{8}$$

and the massless photon condition $K_\mu K^\mu = 0$, we can show that

$$p_4 \cdot K + p_3 \cdot K - p_1 \cdot K - p_2 \cdot K = 0. \tag{9}$$

Thus, we can define a single on-shell point $(\bar{u}, \bar{t})$ [or $(\bar{s}, \bar{t})$] that satisfies the on-shell point condition

$$\bar{s} + \bar{u} + \bar{t} = 4m^2. \tag{10}$$

It should be emphasized that the Mandelstam variables $\bar{s}$, $\bar{u}$, and $\bar{t}$ are all functions of the photon energy $K \neq 0$. This implies that the on-shell point $(\bar{u}, \bar{t})$ is a function of $K \neq 0$. The bremsstrahlung amplitude $M_\mu(\Gamma_\mu; \bar{u}, \bar{t})$ is evaluated at the on-shell point $(\bar{u}, \bar{t})$.

D. The third set: The one on-shell point at the elastic limit $(\tilde{u}, \tilde{t})$

In the elastic limit, the photon energy approaches zero $(K \to 0)$, and all on-shell points $[(u_{32}, t_{42}), (u_{41}, t_{31}), (u_{41}, t_{42}), (u_{32}, t_{31}), (\bar{u}, \bar{t})]$ reduce to the unique on-shell point $(\tilde{u}, \tilde{t})$ [or $(\tilde{s}, \tilde{t})$], which satisfies the on-shell point condition

$$\tilde{s} + \tilde{u} + \tilde{t} = 4m^2. \tag{11}$$

Thus, the bremsstrahlung amplitude $M_\mu(\Gamma_\mu; \tilde{u}, \tilde{t})$ is evaluated at the on-shell point $(\tilde{u}, \tilde{t})$. The on-shell point $(\tilde{u}, \tilde{t})$ is exactly the same as the on-shell point used in the elastic (nonradiative) amplitude. The most important difference between the on-shell point $(\bar{u}, \bar{t})$ [or $(\bar{s}, \bar{t})$] defined in Sec. II C and the on-shell point $(\tilde{u}, \tilde{t})$ [or $(\tilde{s}, \tilde{t})$] defined here is that the point $(\bar{u}, \bar{t})$ is a function of K, whereas the point $(\tilde{u}, \tilde{t})$ is independent of K. Moreover, if both bremsstrahlung amplitudes $M_\mu(\Gamma_\mu; \bar{u}, \bar{t})$ and $M_\mu(\Gamma_\mu; \tilde{u}, \tilde{t})$ are expanded in powers of K, we obtain two different soft-photon expansions:

$$M_\mu(\Gamma_\mu; \bar{u}, \bar{t}) = \frac{A(\bar{u}, \bar{t})}{K} + B(\bar{u}, \bar{t}) + C(\bar{u}, \bar{t})K + \cdots \tag{12}$$

and

$$M_\mu(\Gamma_\mu; \tilde{u}, \tilde{t}) = \frac{A(\tilde{u}, \tilde{t})}{K} + B(\tilde{u}, \tilde{t}) + C(\tilde{u}, \tilde{t})K + \cdots. \tag{13}$$

All coefficients $[A(\bar{u}, \bar{t}), B(\bar{u}, \bar{t}), C(\bar{u}, \bar{t}), \ldots]$ in the first soft-photon expansion given by Eq. (12) are functions of K. However, all coefficients $[A(\tilde{u}, \tilde{t}), B(\tilde{u}, \tilde{t}), C(\tilde{u}, \tilde{t}), \ldots]$ in the second soft-photon expansion given by Eq. (13) are independent of K. This third set of on-shell points plays an important role in the Appendix.

III. ROBE ppy AMPLITUDE

The ROBE approach is based on Horowitz's one-boson-exchange (OBE) model for the two-nucleon scattering amplitude [14]. The Horowitz model, which is an alternative representation of the two-nucleon elastic amplitude, involves a set of OBE parameters determined by fitting directly to the Arndt amplitudes without iteration of the meson exchanges. Thus, the main difference between the standard Goldberger-Grisaru-MacDowell-Wong (GGMW) amplitude [15] and the

Horowitz OBE amplitude is that the GGMW amplitude is expressed in terms of a set of real phase shifts, whereas the Horowitz amplitude is expressed in terms of a set of complex OBE parameters. The GGMW amplitude has been used as input for $pp\gamma$ calculations using the amplitudes $M_\mu^{\rm TuTts}$ and $M_\mu^{\rm Low}$ in the soft-photon approach [3,9,10,12,13,16].

We use the following four different ROBE $pp\gamma$ amplitudes to calculate $pp\gamma$ cross sections:

(i) The detailed expression for the original ROBE $pp\gamma$ amplitude $M_\mu^{\rm PS}(\Gamma_\mu)$ can be found in Ref. [17]. This amplitude is a pseudoscalar (PS) amplitude with the pion-nucleon coupling treated as a PS interaction, and the expression for Γ_μ can be written as

$$\Gamma_\mu = \gamma_\mu - \frac{i\kappa_p}{2m}\sigma_{\mu\nu}K^\nu, \tag{14}$$

where m, κ_p, and K^ν are the proton mass, the proton anomalous magnetic moment, and the photon four-momentum, respectively. (The Bjorken-Drell convention for the metric and the γ matrices is used in our work.) This $M_\mu^{\rm PS}(\Gamma_\mu)$ is used for our four-on-shell-point amplitude $M_\mu^{\rm ROBE}(\Gamma_\mu; u_{41}, u_{32}, t_{31}, t_{42})$,

$$M_\mu^{\rm ROBE}(\Gamma_\mu; u_{41}, u_{32}, t_{31}, t_{42}) \equiv M_\mu^{\rm PS}(\Gamma_\mu). \tag{15}$$

The amplitude $M_\mu^{\rm ROBE}(\Gamma_\mu; u_{41}, u_{32}, t_{31}, t_{42})$ is evaluated at the four different on-shell points defined in Sec. II.

(ii) The one-on-shell-point amplitude is $M_\mu^{\rm ROBE}(\Gamma_\mu; \bar{u}, \bar{t})$, which is obtained from the amplitude $M_\mu^{\rm ROBE}(\Gamma_\mu; u_{41}, u_{32}, t_{31}, t_{42})$ [Eq. (15)] by changing the different t's (t_{31} and t_{42}) to $\bar{t} = (t_{31} + t_{42})/2$ and the different u's (u_{41} and u_{32}) to $\bar{u} = (u_{41} + u_{32})/2$,

$$M_\mu^{\rm ROBE}(\Gamma_\mu; \bar{u}, \bar{t}) \equiv M_\mu^{\rm ROBE}(\Gamma_\mu; u_{41} \to \bar{u}, u_{32} \to \bar{u}, t_{31} \to \bar{t}, t_{42} \to \bar{t}). \tag{16}$$

Thus, the amplitude $M_\mu^{\rm ROBE}(\Gamma_\mu; \bar{u}, \bar{t})$ is evaluated at one on-shell-point $(\bar{u}, \bar{t})$. Because the derivation of the amplitude $M_\mu^{\rm ROBE}(\Gamma_\mu; \bar{u}, \bar{t})$ differs from the derivation of the Low amplitude $M_\mu^{\rm Low}(\Gamma_\mu; \bar{u}, \bar{t})$, the two amplitudes are not the same and may predict somewhat different $pp\gamma$ cross sections.

(iii) We can define an amplitude $\bar{M}_\mu^{\rm ROBE}(\kappa_p = 0)$, which does not involve the κ_p contribution, by setting $\Gamma_\mu = (\Gamma_\mu)_{\kappa_p=0} = \gamma_\mu$, such that

$$\bar{M}_\mu^{\rm ROBE}(\kappa_p = 0) \equiv M_\mu^{\rm ROBE}(\Gamma_\mu = \gamma_\mu; u_{41}, u_{32}, t_{31}, t_{42}). \tag{17}$$

(iv) We can define an amplitude $\bar{M}_\mu^{\rm ROBE}(\kappa_p$ alone), which involves the contribution from κ_p only, by setting $\Gamma_\mu = -\frac{i\kappa_p}{2m}\sigma_{\mu\nu}K^\nu$, such that

$$\bar{M}_\mu^{\rm ROBE}(\kappa_p \text{ alone}) \equiv \bar{M}_\mu^{\rm ROBE}\left(\Gamma_\mu = -\frac{i\kappa_p}{2m}\sigma_{\mu\nu}K^\mu; u_{41}, u_{32}, t_{31}, t_{42}\right). \tag{18}$$

All of these four amplitudes [$M_\mu^{\rm ROBE}(\Gamma_\mu; u_{41}, u_{32}, t_{31}, t_{42})$, $\bar{M}_\mu^{\rm ROBE}(\Gamma_\mu; \bar{u}, \bar{t})$, $\bar{M}_\mu^{\rm ROBE}(\kappa_p = 0)$, $\bar{M}_\mu^{\rm ROBE}(\kappa_p$ alone)] are gauge invariant, and they obey the soft-photon theorem. Because they are either defined or derived from the original pseudoscalar amplitude $M_\mu^{\rm PS}(\Gamma_\mu)$, they are all pseudoscalar amplitudes. The reasons for using the amplitude $M_\mu^{\rm PS}(\Gamma_\mu)$ in this investigation are the following: (i) As shown in Ref. [18], the PS amplitude $M_\mu^{\rm PS}(\Gamma_\mu)$ and the pseudovector (PV) amplitude $M_\mu^{\rm PV}(\Gamma_\mu)$ predict quantitatively similar $pp\gamma$ cross sections at 190 MeV. Most of these predicted cross sections are in excellent agreement with the high-precision KVI data. In other words, the precise KVI cross-section data cannot be used to differentiate between the PS and PV $pp\gamma$ amplitudes. (ii) As shown in Figs. 1–5, the amplitude $M_\mu^{\rm PS}(\Gamma_\mu)$ and the TuTts soft-photon amplitude $M_\mu^{\rm TuTts}$ have very similar predictive power in the kinematic region investigated. This fact provides the best verification of the validity of the amplitude $M_\mu^{\rm PS}(\Gamma_\mu)$, because the amplitude $M_\mu^{\rm TuTts}$ has already been thoroughly tested and its validity in describing existing data has been well established. (iii) Because the amplitude $M_\mu^{\rm TuTts}$ is pseudoscalar in nature, it is more meaningful to compare the amplitude $M_\mu^{\rm PS}(\Gamma_\mu)$ with the amplitude $M_\mu^{\rm TuTts}$.

IV. $pp\gamma$ CROSS SECTION AND COMPARISON BETWEEN THEORY AND EXPERIMENT

All four $pp\gamma$ amplitudes [$M_\mu^{\rm ROBE}(\Gamma_\mu; u_{41}, u_{32}, t_{31}, t_{42})$, $M_\mu^{\rm ROBE}(\Gamma_\mu; \bar{u}, \bar{t})$, $\bar{M}_\mu^{\rm ROBE}(\kappa_p = 0)$, $\bar{M}_\mu^{\rm ROBE}(\kappa_p$ alone)] were used to calculate $pp\gamma$ cross sections $d^3\sigma/d\Omega_3 d\Omega_4 d\psi_\gamma$ as functions of the photon angle ψ_γ at 190 and 280 MeV. Selected

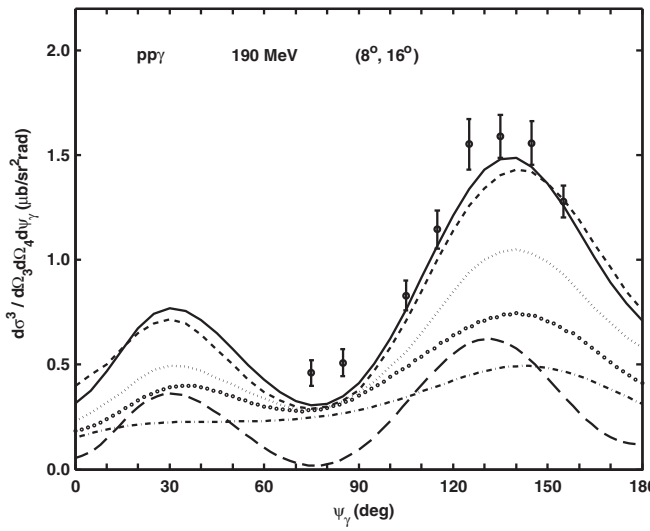

FIG. 1. Coplanar $pp\gamma$ cross sections as a function of the photon angle ψ_γ at 190 MeV for the proton scattering angles $(\theta_3, \theta_4) = (8^\circ, 16^\circ)$. The solid, short-dashed, dotted, circled, long-dashed, and dot-dashed curves are calculated using amplitudes $M_\mu^{\rm ROBE}(\Gamma_\mu; u_{41}, u_{32}, t_{31}, t_{42})$, $M_\mu^{\rm TuTts}(\Gamma_\mu; u_{41}, u_{32}, t_{31}, t_{42})$, $M_\mu^{\rm Low}(\Gamma_\mu; \bar{u}, \bar{t})$, $M_\mu^{\rm ROBE}(\Gamma_\mu; \bar{u}, \bar{t})$, $\bar{M}_\mu^{\rm ROBE}(\kappa_p = 0)$, and $\bar{M}_\mu^{\rm ROBE}(\kappa_p$ alone), respectively. The experimental data are from Refs. [4–7].

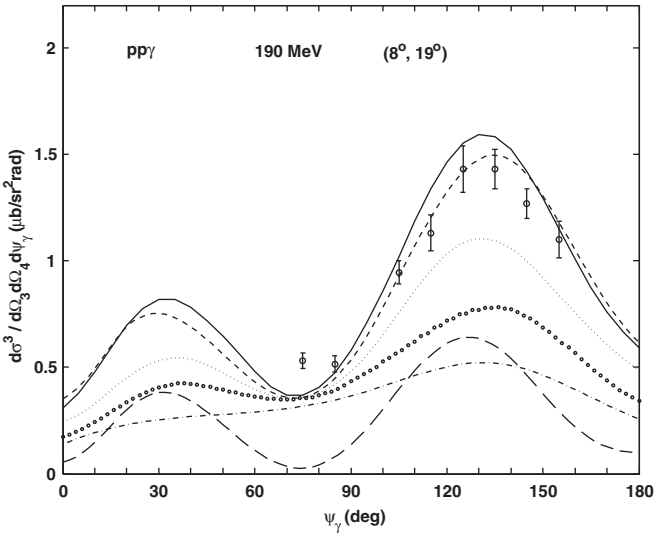

FIG. 2. The same as Fig. 1, but for the proton scattering angles $(\theta_3, \theta_4) = (8^\circ, 19^\circ)$.

results are exhibited in five figures. Figures 1, 2, and 3 show calculated cross sections at 190 MeV. Figures 4 and 5 display calculated cross sections at 280 MeV. The scattering angles (θ_3, θ_4) are $(8^\circ, 16^\circ)$ for Fig. 1, $(8^\circ, 19^\circ)$ for Fig. 2, $(16^\circ, 19^\circ)$ for Fig. 3, $(12^\circ, 12.4^\circ)$ for Fig. 4, and $(28^\circ, 12.4^\circ)$ for Fig. 5. The calculated cross sections at 190 MeV are compared with the KVI data [4–7], whereas the calculated cross sections at 280 MeV are compared with the TRIUMF data [8]. To demonstrate that some important features observed in Refs. [9,10] (based on calculations using the $pp\gamma$ TuTts amplitude and the Low amplitude) can also be found in our ROBE calculations using the amplitudes $M_\mu^{\rm ROBE}(\Gamma_\mu; u_{41}, u_{32}, t_{31}, t_{42})$ and $M_\mu^{\rm ROBE}(\Gamma_\mu; \bar{u}, \bar{t})$, we include the two additional calculations using the amplitude $M_\mu^{\rm TuTts}(\Gamma_\mu; u_{41}, u_{32}, t_{31}, t_{42})$ and the Low amplitude $M_\mu^{\rm Low}(\Gamma_\mu; \bar{u}, \bar{t})$ in all five figures. Thus, there are six different $pp\gamma$ curves in each of the five figures.

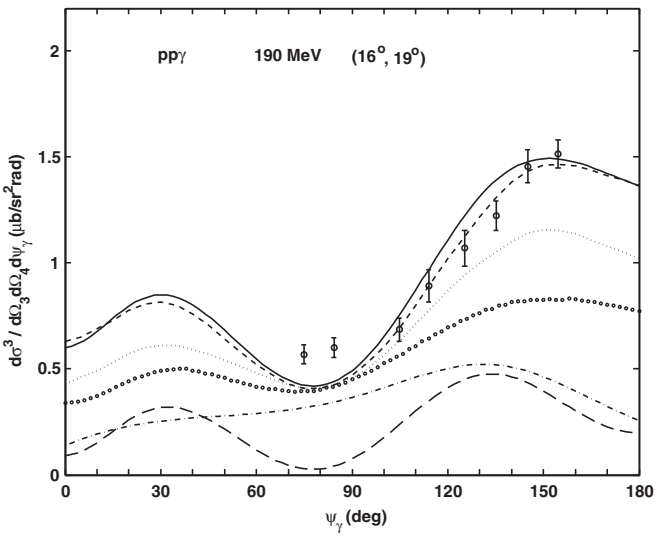

FIG. 3. The same as Fig. 1, but for the proton scattering angles $(\theta_3, \theta_4) = (16^\circ, 19^\circ)$.

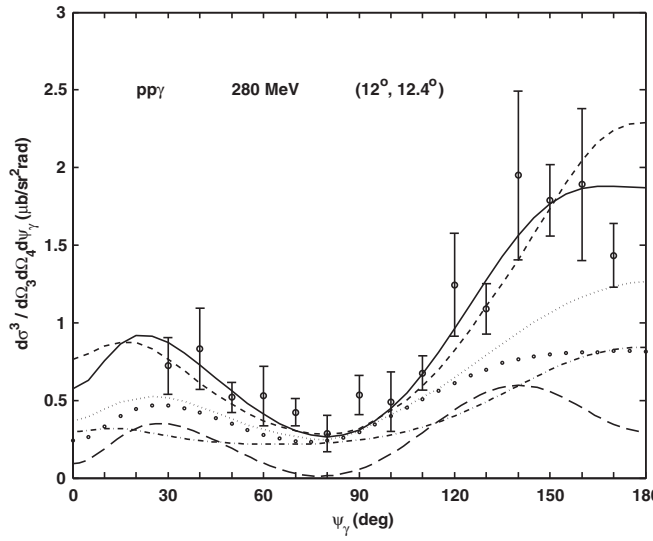

FIG. 4. The same as Fig. 1, but at 280 MeV for the proton scattering angles $(\theta_3, \theta_4) = (12^\circ, 12.4^\circ)$, and with experimental data from Ref. [8].

In each figure, the solid curve corresponds to the ROBE amplitude $M_\mu^{\rm ROBE}(\Gamma_\mu; u_{41}, u_{32}, t_{31}, t_{42})$. The circled curve corresponds to the ROBE amplitude $M_\mu^{\rm ROBE}(\Gamma_\mu; \bar{u}, \bar{t})$. The long-dashed curve corresponds to the ROBE amplitude $\bar{M}_\mu^{\rm ROBE}(\kappa_p = 0)$. The dot-dashed curve corresponds to the ROBE amplitude $\bar{M}_\mu^{\rm ROBE}(\kappa_p$ alone). The short-dashed curve corresponds to the TuTts amplitude $M_\mu^{\rm TuTts}(\Gamma_\mu; u_{41}, u_{32}, t_{31}, t_{42})$. The dotted curve corresponds to the Low amplitude $M_\mu^{\rm Low}$. The TuTts (short-dashed) curves and the Low (dotted) curves are from Ref. [10]. Note that the complete expression for Low's $pp\gamma$ amplitude, which was first derived by Nyman [11] using Low's prescription [1], can be found in Ref. [10].

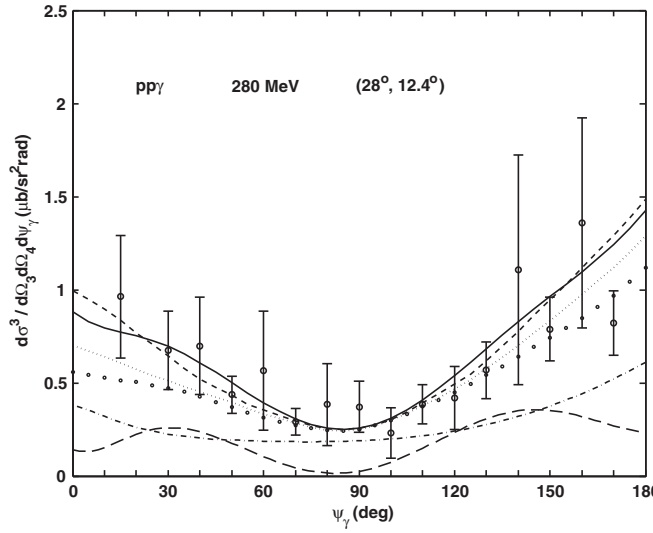

FIG. 5. The same as Fig. 1, but at 280 MeV for the proton scattering angles $(\theta_3, \theta_4) = (28^\circ, 12.4^\circ)$, and with experimental data from Ref. [8].

On the basis of the theoretical calculations and experimental measurements illustrated in Figs. 1–5, we summarize the following significant features:

(i) The solid curves are consistently in close agreement with the short-dashed curves. More examples of such an agreement at 190 MeV can be found in Ref. [18]. This strongly suggests that the two amplitudes, $M_\mu^{\mathrm{ROBE}}(\Gamma_\mu; u_{41}, u_{32}, t_{31}, t_{42})$ and $M_\mu^{\mathrm{TuTts}}(\Gamma_\mu; u_{41}, u_{32}, t_{31}, t_{42})$, have very similar predictive power in the kinematic region investigated (190–280 MeV). Furthermore, these two calculations are in much better agreement with the KVI and TRIUMF data than are the dotted and circled curves. Thus, the $M_\mu^{\mathrm{ROBE}}(\Gamma_\mu; u_{41}, u_{32}, t_{31}, t_{42})$ and $M_\mu^{\mathrm{TuTts}}(\Gamma_\mu; u_{41}, u_{32}, t_{31}, t_{42})$ amplitudes, which are four-on-shell-point amplitudes, describe the KVI and TRIUMF data much better than do the $M_\mu^{\mathrm{Low}}(\Gamma_\mu; \bar{u}, \bar{t})$ and $M_\mu^{\mathrm{ROBE}}(\Gamma_\mu; \bar{u}, \bar{t})$ amplitudes, which are one-on-shell-point amplitudes. As discussed in Ref. [9], this is because the four-on-shell-point models retain almost all of the important contributions from the κ_p-dependent terms. We emphasize that even though the two different one-on-shell-point amplitudes, $M_\mu^{\mathrm{Low}}(\Gamma_\mu; \bar{u}, \bar{t})$ and $M_\mu^{\mathrm{ROBE}}(\Gamma_\mu; \bar{u}, \bar{t})$, can be defined, neither of them can be used to describe the experimental data shown in the five figures.

(ii) When we compare the long-dashed curves and the dot-dashed curves with the KVI and TRIUMF data, we see that neither the amplitude $\bar{M}_\mu^{\mathrm{ROBE}}(\kappa_p = 0)$ nor the amplitude $\bar{M}_\mu^{\mathrm{ROBE}}(\kappa_p$ alone) satisfactorily describe the data. That is, neither photon emission from charge scattering nor photon emission from magnetic moment scattering is dominant in the $pp\gamma$ process.

(iii) Generally, the contribution from κ_p was investigated by comparing the solid (or short-dashed) curve with the long-dashed curve. At a given angle ψ_γ, the difference in cross section between the solid (or short-dashed) curve and the long-dashed curve provides an estimate of the κ_p contribution. A large difference means the κ_p contribution is significant, whereas a small difference is interpreted to mean an insignificant contribution. Using the size difference found in Figs. 1–5 as an example, the κ_p contribution is quite significant in this case, but nevertheless it does not completely dominate the cross section. To examine to what degree it can be said that the κ_p contribution dominates the $pp\gamma$ cross section, we must also examine the dot-dashed curve calculated using the amplitude $\bar{M}_\mu^{\mathrm{ROBE}}(\kappa_p$ alone). If the contribution from κ_p completely dominates the cross section at a given ψ_γ, it must satisfy two conditions: (i) the long-dashed curve at ψ_γ must be nearly zero and (ii) the dot-dashed curve at ψ_γ must be very close to the solid curve. On the basis of these two requirements, we conclude that the κ_p contribution completely dominates the $pp\gamma$ cross sections (shown in Figs. 1–5) only in the vicinity of $\psi_\gamma = 75^\circ$.

V. THE EFFECT OF DIFFERENT ON-SHELL-POINT CONDITIONS ON THE $pp\gamma$ CROSS SECTION

In Refs. [9,10] it was established that the four-on-shell-point TuTts amplitude and the one-on-shell-point Low amplitude led to significantly different results corresponding to the 190-MeV KVI data. Here we use the ROBE amplitudes to investigate the effect on the $pp\gamma$ cross section of using different on-shell-point conditions. Using a different approach allows us to demonstrate that the effect is independent of the bremsstrahlung approach used for the investigation. Furthermore, we search for general principles that govern the effect of different on-shell-point conditions on the $pp\gamma$ cross section. Such general principles are applicable to other bremsstrahlung processes involving the scattering of two identical nucleons (such as $nn\gamma$, $pp\nu\bar{\nu}$, and $nn\nu\bar{\nu}$). The amplitude $M_\mu^{\mathrm{ROBE}}(\Gamma_\mu; u_{41}, u_{32}, t_{31}, t_{42})$ given by Eq. (15) and the amplitude $M_\mu^{\mathrm{ROBE}}(\Gamma_\mu; \bar{u}, \bar{t})$ given by Eq. (16) are used as the four-on-shell-point amplitude and the one-on-shell-point amplitude, respectively, in our investigation. Both $M_\mu^{\mathrm{ROBE}}(\Gamma_\mu; u_{41}, u_{32}, t_{31}, t_{42})$ and $M_\mu^{\mathrm{ROBE}}(\Gamma_\mu; \bar{u}, \bar{t})$ are gauge-invariant amplitudes. These two amplitudes were used to calculate $pp\gamma$ cross sections as a function of ψ_γ at several proton incident energies E_i for various symmetric proton scattering angles $\theta = \theta_3 = \theta_4$. Selected $pp\gamma$ cross-section results are shown in Fig. 6(a) (at $E_i =$ 50 MeV for $\theta = 10^\circ, 40^\circ, 42^\circ, 43^\circ$) and Fig. 7(a) (at $E_i =$ 190 MeV for $\theta = 10^\circ, 40^\circ, 42^\circ, 43^\circ$). In both figures, the solid curves are calculated using the four-on-shell-point amplitude $M_\mu^{\mathrm{ROBE}}(\Gamma_\mu; u_{41}, u_{32}, t_{31}, t_{42})$ and the dashed curves are calculated using the one-on-shell-point amplitude $M_\mu^{\mathrm{ROBE}}(\Gamma_\mu; \bar{u}, \bar{t})$. The effect on the $pp\gamma$ cross section of using the two different on-shell-point conditions can be measured by the ratio $R_{\psi_\gamma}^{E_i}(\theta)$ as a function of the proton scattering angle $\theta = \theta_3 = \theta_4$. For a given incident proton energy E_i and the angle θ, as shown in Figs. 6(a) and 7(a), both the solid curve and the dashed curve can be calculated as a function of ψ_γ. The ratio $R_{\psi_\gamma}^{E_i}(\theta)$ is defined as

$$R_{\psi_\gamma}^{E_i}(\theta) = \frac{\begin{pmatrix}\text{value of cross section at } \psi_\gamma \text{ calculated} \\ \text{from the four-on-shell-point amplitude}\end{pmatrix}}{\begin{pmatrix}\text{value of cross section at } \psi_\gamma \text{ calculated} \\ \text{from the one-on-shell-point amplitude}\end{pmatrix}}. \tag{19}$$

To demonstrate that the ratio $R_{\psi_\gamma}^{E_i}(\theta)$ depends also on the photon energy K, we calculate K as a function of ψ_γ, $K(\psi_\gamma)$, for two cases: (1) Figure 6(b) shows the results for $K(\psi_\gamma)$ at $E_i = 50$ MeV for $\theta = 10^\circ, 40^\circ, 42^\circ$, and 43°. These results, combined with those from Fig. 6(a), determine the values of the ratio $R_{\psi_\gamma}^{E_i}(\theta)$ and their corresponding values of K at any ψ_γ angle. (2) Figure 7(b) shows the results for $K(\psi_\gamma)$ at $E_i = 190$MeV for $\theta = 10^\circ, 40^\circ, 42^\circ$, and 43°. Combining Fig. 7(b) with Fig. 7(a), the values of the ratio $R_{\psi_\gamma}^{E_i}(\theta)$ and their corresponding values of K at any ψ_γ angle can be determined.

The following are important features:

(i) As discussed regarding Figs 1–5, the two four-on-shell-point amplitudes $M_\mu^{\mathrm{ROBE}}(\Gamma_\mu; u_{41}, u_{32}, t_{31}, t_{42})$

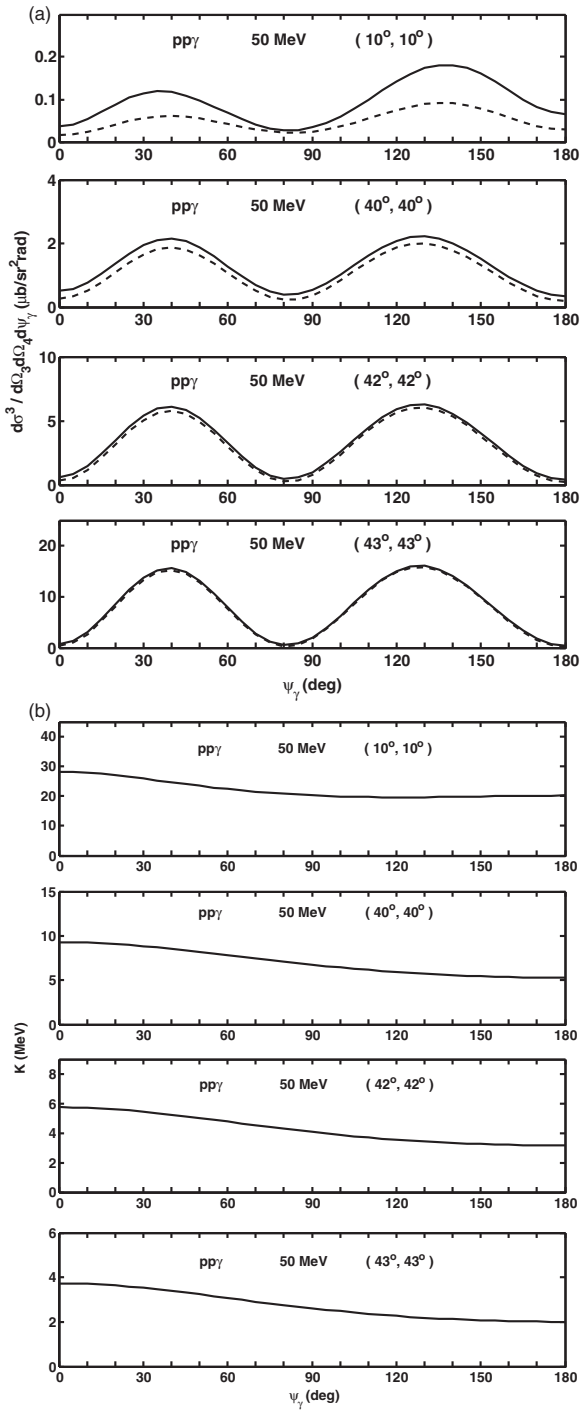

FIG. 6. (a) Coplanar $pp\gamma$ cross sections as a function of ψ_γ at 50 MeV for the proton scattering angles $(\theta_3, \theta_4) = (10^\circ, 10^\circ)$, $(40^\circ, 40^\circ)$, $(42^\circ, 42^\circ)$, and $(43^\circ, 43^\circ)$. All solid curves are calculated using the four-on-shell-point amplitude $M_\mu^{\mathrm{ROBE}}(\Gamma_\mu; u_{41}, u_{32}, t_{31}, t_{42})$, while all dashed curves are calculated using the one-on-shell-point amplitude $M_\mu^{\mathrm{ROBE}}(\Gamma_\mu; \bar{u}, \bar{t})$. (b) The photon energy K as a function of ψ_γ at 50 MeV for the proton scattering angles $(\theta_3, \theta_4) = (10^\circ, 10^\circ)$, $(40^\circ, 40^\circ)$, $(42^\circ, 42^\circ)$, and $(43^\circ, 43^\circ)$.

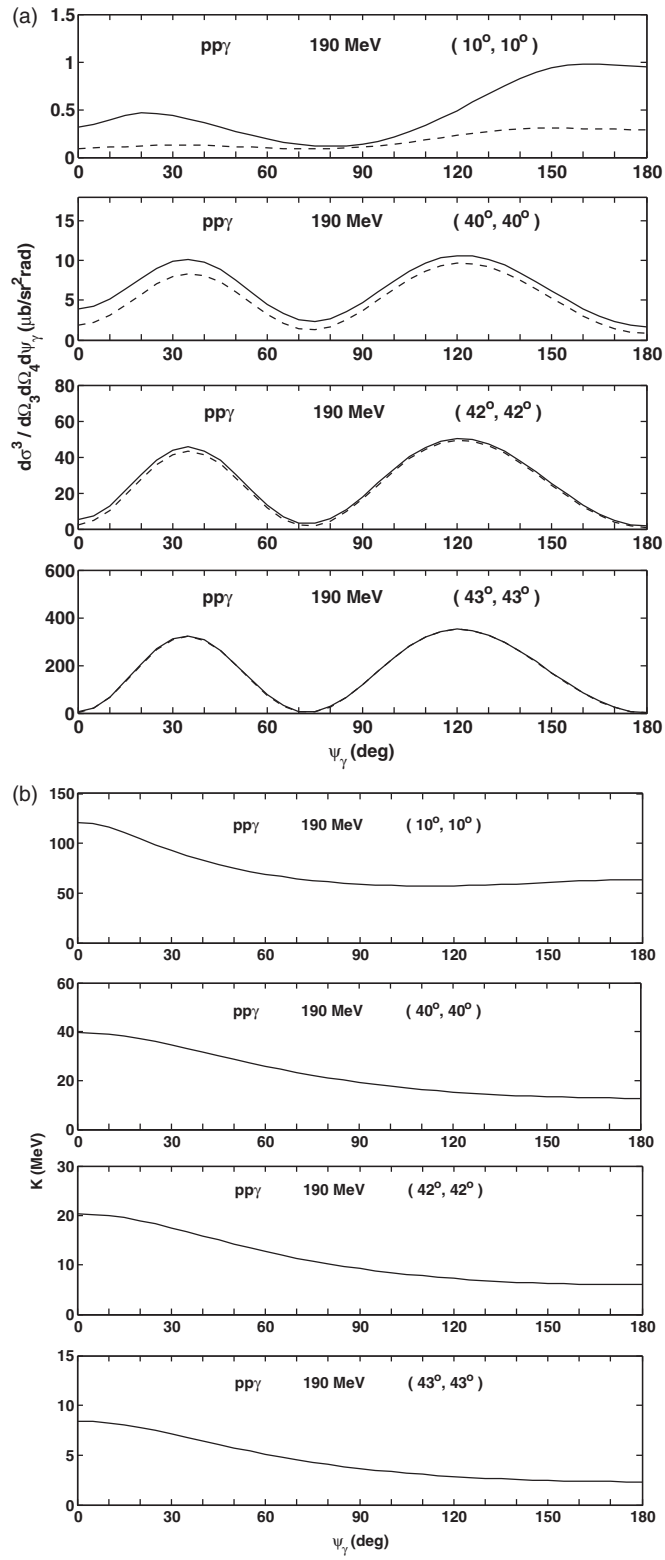

FIG. 7. (a) The same as Fig. 6(a), but for the incident energy 190 MeV. (b) The same as Fig. 6(b), but for the incident energy 190 MeV.

and M_μ^{TuTts} provide similar predictive power in the kinematic region investigated, and they can be used to describe both the KVI and the TRIUMF data.

(ii) The different on-shell-point conditions affect the $pp\gamma$ cross section sensitively as a function of the scattering angle θ. In the range $0 \leqslant \theta < 45^\circ$, the size of the effect

TABLE I. $R_{\psi_\gamma}^{E_i}$ as a function of θ or K at the incident proton energies E_i of 50 and 190 MeV for the photon emission angles ψ_γ of 30° and 150°. E_i, ψ_γ, θ, $d^3\sigma/d\Omega_3 d\Omega_4 d\psi_\gamma$, and K are the incident energies, the photon emission angles, the proton scattering angles, the $pp\gamma$ cross sections, and the photon energies, respectively.

			$d^3\sigma/d\omega_3 d\omega_4 d\psi_y$ (μb/sr^2 rad)			
E_i (MeV)	ψ_y	θ ($\theta_3 = \theta_4$)	Four-on-shell-point	One-on-shell-point	$R_{\psi_y}^{E_i}(\theta)$ or $R_{\psi_y}^{E_i}(K)$	K (MeV)
50	30°	10°	0.11	0.06	1.83	25.93
		40°	1.95	1.65	1.18	8.83
		42°	5.41	5.05	1.07	5.45
		43°	13.75	13.36	1.03	3.53
	150°	10°	0.16	0.08	2.00	19.91
		40°	1.52	1.31	1.16	5.45
		42°	4.02	3.80	1.06	3.26
		43°	10.00	9.77	1.02	2.07
190	30°	10°	0.44	0.13	3.38	92.99
		40°	9.89	7.99	1.24	34.65
		42°	43.64	41.35	1.06	17.51
		43°	310.54	308.02	1.01	7.16
	150°	10°	0.94	0.31	3.03	60.61
		40°	6.16	5.25	1.17	13.36
		42°	25.36	24.47	1.04	6.26
		43°	169.74	168.88	1.01	2.45

increases as θ decreases. In other words, the effect is more significant for small angle scattering ($\theta \leqslant 10°$), and it becomes less significant as the angle tends to the elastic limit ($\theta \to 45°$). This can be seen from Figs. 6(a) and 7(a). To demonstrate this fact quantitatively, we show in Table I the numerical values of the cross sections calculated using both the four-on-shell-point amplitude $M_\mu^{\mathrm{ROBE}}(\Gamma_\mu; u_{41}, u_{32}, t_{31}, t_{42})$ given by Eq. (15) and the one-on-shell-point amplitude $\bar{M}_\mu^{\mathrm{ROBE}}(\Gamma_\mu; \bar{u}, \bar{t})$ given by Eq. (16) at $E_i = 50$ and 190 MeV for $\psi_\gamma = 30°$ and 150° and $\theta = 10°, 40°, 42°$, and 43°. We also show the calculated values of the ratio $R_{\psi_\gamma}^{E_i}(\theta)$ and their corresponding photon energies K for all cases. There are four sets of (E_i, ψ_γ) [(50 MeV, 30°), (50 MeV, 150°), (190 MeV, 30°), (190 MeV, 150°)] and each set involves four different θ angles ($\theta = 10°, 40°, 42°, 43°$). From Table I, one sees that the ratio $R_{\psi_\gamma}^{E_i}(\theta)$ attains its largest value at $\theta = \theta_3 = \theta_4 = 10°$ (in the small angle scattering region), and it attains its smallest value, approaching 1, at $\theta = 43°$ (in the region of the elastic limit). In fact, we can show numerically that

$$\lim_{\theta \to 45°} R_{\psi_\gamma}^{E_i}(\theta) = 1 \tag{20}$$

at any ψ_γ angle. This overall behavior is universal, independent of the incident energy E_i, as illustrated in Figs. 6(a) and 7(a).

(iii) It is clear from Table I (or a comparison of Fig. 6(a) [Fig. 7(a)] with Fig. 6(b) [Fig. 7(b)]) that the ratio $R_{\psi_\gamma}^{E_i}$ also depends sensitively on the photon energy K. The ratio $R_{\psi_\gamma}^{E_i}$ decreases as the photon energy decreases. The following relationship can be established. The small angle scattering region ($\theta < 10°$) is equivalent to the hard-photon region ($K > 25.9$ MeV for $E_i = 50$ MeV at $\psi_\gamma = 30°$ and $K > 92$ MeV for $E_i = 190$ MeV at $\psi_\gamma = 30°$), and the region of the elastic limit ($43° \leqslant \theta < 45°$) is equivalent to the low photon energy region ($K < 4$ MeV for $E_i = 50$ MeV at $\psi_\gamma = 30°$ and $K < 7.2$ MeV for $E_i = 190$ MeV at $\psi_\gamma = 30°$). Thus, the ratio $R_{\psi_\gamma}^{E_i}$ can be written either as a function of θ or as a function of K, i.e., $R_{\psi_\gamma}^{E_i}(\theta)$ or $R_{\psi_\gamma}^{E_i}(K)$. In the Appendix, we prove that

$$\lim_{K \to 0} R_{\psi_\gamma}^{E_i}(K) = 1. \tag{21}$$

Thus, we have

$$\lim_{\theta \to 45°} R_{\psi_\gamma}^{E_i}(\theta) = \lim_{K \to 0} R_{\psi_\gamma}^{E_i}(K) = 1. \tag{22}$$

(iv) An important implication of our investigation is that the one-on-shell-point $pp\gamma$ amplitudes are valid only in the region of the elastic limit.

VI. CONCLUSION

We demonstrated a quantitative understanding of the $pp\gamma$ process. The ROBE four-on-shell-point amplitude, which predicts cross sections in quantitative agreement with the soft-photon TuTts amplitude, can be used to describe precision $pp\gamma$ data such as those from KVI. In the hard-photon region, the ROBE four-on-shell-point amplitude is essential for a proper description of the data. Only near the elastic limit does the one-on-shell-point approximation approach the four-on-shell-point result. For this reason the one-on-shell-point ROBE amplitude and the Low soft-photon amplitude fail to describe the KVI data but do provide an adequate description at much lower photon energy. Moreover, an

important photon emission mechanism involves the nucleon anomalous magnetic moment, although it does not completely dominate the cross section.

ACKNOWLEDGMENTS

M. K. Liou and B. F. Gibson thank R. G. E. Timmermans for the TuTts $pp\gamma$ cross sections presented in Figs. 1–5. Numerical results in this paper were performed on the supercomputer of the CUNY High Performance Computing Center situated at the College of Staten Island. The work of Y. Li was supported by a grant from Guangxi University, the work of M. K. Liou and W. M. Schreiber was supported in part by the CUNY Professional Staff Congress-Board of Higher Education Research Award Program, and the work of B. F. Gibson was carried out under the auspices of the National Nuclear Security Administration of the US Department of Energy at Los Alamos National Laboratory under Contract No. DEAC52-06NA25396.

APPENDIX: PROOF THAT $\lim_{K\to 0} R^{E_i}_{\psi_\gamma}(K) = 1$

Consider the $pp\gamma$ process

$$p\left(p_1^\mu\right) + p\left(p_2^\mu\right) \to p\left(p_3^\mu\right) + p\left(p_4^\mu\right) + \gamma(K^\mu), \tag{A1}$$

where p_1^μ (p_3^μ) and p_2^μ (p_4^μ) are the initial (final) four-momenta of the two interacting protons, and K^μ is the four-momentum of the emitted photon. These four-momenta satisfy the energy-momentum conservation relation

$$p_1^\mu + p_2^\mu = p_3^\mu + p_4^\mu + K^\mu. \tag{A2}$$

In the limit that K approaches zero, the $pp\gamma$ process reduces to the corresponding pp elastic scattering process,

$$p\left(p_1^\mu\right) + p\left(p_2^\mu\right) \to p\left(\tilde{p}_3^\mu\right) + p\left(\tilde{p}_4^\mu\right), \tag{A3}$$

where

$$\begin{aligned} \tilde{p}_3^\mu &= \lim_{K\to 0} p_3^\mu, \\ \tilde{p}_4^\mu &= \lim_{K\to 0} p_4^\mu. \end{aligned} \tag{A4}$$

The energy-momentum conservation relation becomes

$$p_1^\mu + p_2^\mu = \tilde{p}_3^\mu + \tilde{p}_4^\mu, \tag{A5}$$

which can also be written as

$$p_1^\mu - \tilde{p}_3^\mu = -\left(p_2^\mu - \tilde{p}_4^\mu\right) \tag{A6}$$

and

$$p_1^\mu - \tilde{p}_4^\mu = -\left(p_2^\mu - \tilde{p}_3^\mu\right). \tag{A7}$$

Equations (A4) and (A6) give

$$\lim_{K\to 0} t_{13} = \lim_{K\to 0}(p_1 - p_3)^2 = (p_1 - \tilde{p}_3)^2 \equiv \tilde{t}, \tag{A8}$$

$$\lim_{K\to 0} t_{24} = \lim_{K\to 0}(p_2 - p_4)^2 = (p_2 - \tilde{p}_4)^2 = (p_1 - \tilde{p}_3)^2 = \tilde{t}, \tag{A9}$$

$$\lim_{K\to 0} \bar{t} = \lim_{K\to 0} (t_{13} + t_{24})\, 2 = \tilde{t}. \tag{A10}$$

Equations (A4) and (A7) give

$$\lim_{K\to 0} u_{14} = (p_1 - \tilde{p}_4)^2 \equiv \tilde{u}, \tag{A11}$$

$$\lim_{K\to 0} u_{23} = (p_1 - \tilde{p}_4)^2 = \tilde{u}, \tag{A12}$$

$$\lim_{K\to 0} \bar{u} = \lim_{K\to 0} (u_{14} + u_{23})/2 = \tilde{u}. \tag{A13}$$

We also have

$$\lim_{K\to 0} s_f = (p_3 + p_4)^2 = (\tilde{p}_3 + \tilde{p}_4)^2 = (p_1 + p_2)^2 = s_i \equiv \tilde{s}, \tag{A14}$$

$$\lim_{K\to 0} \bar{s} = \lim_{K\to 0} (s_f + s_i)/2 = \tilde{s}, \tag{A15}$$

$$\lim_{K\to 0} s_{21} = \lim_{K\to 0} s_{12} = \lim_{K\to 0} s_{22} = \lim_{K\to 0} s_{11} = \tilde{s}. \tag{A16}$$

From Eqs. (A8)–(A16) we can show that all equations given by Eqs. (3a), (3b), (3c), (3d), and (10) reduce to the same identical on-shell condition [Eq. (11)]

$$\tilde{s} + \tilde{t} + \tilde{u} = 4m^2 \tag{A17}$$

in the limit that $K \to 0$. Furthermore, we also find

$$\lim_{K\to 0} M_\mu^{\mathrm{ROBE}}(\Gamma_\mu; u_{41}, u_{32}, t_{31}, t_{42}) = M_\mu^{\mathrm{ROBE}}(\Gamma_\mu; \tilde{u}, \tilde{t}) \tag{A18}$$

and

$$\lim_{K\to 0} M_\mu^{\mathrm{ROBE}}(\Gamma_\mu; \bar{u}, \bar{t}) = M_\mu^{\mathrm{ROBE}}(\Gamma_\mu; \tilde{u}, \tilde{t}). \tag{A19}$$

That is, in the limit that K tends to zero, the four-on-shell-point amplitude is exactly equal to the one-on-shell-point amplitude. Therefore, the cross sections calculated from these two equal amplitudes are the same in this limit, and we have

$$\lim_{K\to 0} R^{E_i}_{\psi_\gamma}(K) = 1,$$

independent of E_i and ψ_γ.

It is important to emphasize that the photon energy K can approach zero only when θ tends to the elastic limit value of 45°, because K is not an independent variable for the H-type cross sections [19]. As discussed in Ref. [19], the cross section $d^3\sigma/d\Omega_3 d\Omega_4 d\psi_\gamma$ is defined as an H-type cross section because the set of five independent variables for this type of cross section is $(\theta_3, \phi_3, \theta_4, \phi_4, \psi_\gamma)$. The photon energy K, which is not an independent variable, can be determined by solving the four energy-momentum conservation equations. In other words, K can be calculated if a set of five variables $(\theta_3, \phi_3, \theta_4, \phi_4, \psi_\gamma)$ and the incident proton energy E_i are given. As shown in Ref. [19], except for the elastic limit case, K cannot be zero for an H-type cross section. If we were to arbitrarily set K equal to zero, then the required condition $p_1^\mu + p_2^\mu - p_3^\mu - p_4^\mu - K^\mu = 0$ is not satisfied, and this would imply that $\delta^4(p_1 + p_2 - p_3 - p_4 - K) = 0$. Because the expression for the cross section involves a factor $\delta^4(p_1 + p_2 - p_3 - p_4 - K)$ (see, for example, Eq. (45) or Eq. (52) of Ref. [19]), the cross section $d^3\sigma/d\Omega_3 d\Omega_4 d\psi_\gamma$ would be zero because $\delta^4(p_1 + p_2 - p_3 - p_4 - K) = 0$. Thus, K can approach zero ($K \to 0$) only when the $pp\gamma$ process approaches its elastic limit ($\theta = \theta_3 = \theta_4 = 45°$).

[1] F. E. Low, Phys. Rev. **110**, 974 (1958).
[2] S. L. Adler and Y. Dothan, Phys. Rev. **151**, 1267 (1966).
[3] R. G. E. Timmermans, B. F. Gibson, Y. Li, and M. K. Liou, Phys. Rev. C **65**, 014001 (2001).
[4] H. Huisman *et al.*, Phys. Rev. Lett. **83**, 4017 (1999).
[5] H. Huisman *et al.*, Phys. Lett. B **476**, 9 (2000).
[6] H. Huisman *et al.*, Phys. Rev. C **65**, 031001 (2002).
[7] M. Mahjour-Shafiei *et al.*, Phys. Rev. C **70**, 024004 (2004).
[8] K. Michaelian *et al.*, Phys. Rev. D **41**, 2689 (1990).
[9] M. K. Liou, T. D. Penninga, R. G. E. Timmermans, and B. F. Gibson, Phys. Rev. C **69**, 011001 (2004).
[10] R. G. E. Timmermans, T. D. Penninga, B. F. Gibson, and M. K. Liou, Phys. Rev. C **73**, 034006 (2006).
[11] E. M. Nyman, Phys. Rev. **170**, 1628 (1968).
[12] M. K. Liou, R. Timmermans, and B. F. Gibson, Phys. Rev. C **54**, 1574 (1996).
[13] M. K. Liou, R. Timmermans, and B. F. Gibson, Phys. Lett. B **345**, 372 (1995); **355**, 606(E) (1995).
[14] C. J. Horowitz, Phys. Rev. C **31**, 1340 (1985).
[15] M. L. Goldberger, M. T. Grisaru, S. W. MacDowell, and D. Y. Wong, Phys. Rev. **120**, 2250 (1960).
[16] Y. Li, M. K. Liou, R. Timmermans, and B. F. Gibson, Phys. Rev. C **58**, R1880 (1998).
[17] Y. Li, M. K. Liou, and W. M. Schreiber, Phys. Rev. C **57**, 507 (1998).
[18] Y. Li, M. K. Liou, and W. M. Schreiber, Phys. Rev. C **72**, 024005 (2005).
[19] M. K. Liou, Phys. Rev. D **18**, 3390 (1978).